Crystal structure of a quinoenzyme: copper amine oxidase of *Escherichia coli* at 2 Å resolution

MR Parsons, MA Convery, CM Wilmot, KDS Yadav†, V Blakeley, AS Corner, SEV Phillips, MJ McPherson and PF Knowles*

Department of Biochemistry and Molecular Biology, University of Leeds, Leeds, LS2 9JT, UK

Background: Copper amine oxidases are a ubiquitous and novel group of quinoenzymes that catalyze the oxidative deamination of primary amines to the corresponding aldehydes, with concomitant reduction of molecular oxygen to hydrogen peroxide. The enzymes are dimers of identical 70–90 kDa subunits, each of which contains a single copper ion and a covalently bound cofactor formed by the post-translational modification of a tyrosine side chain to 2,4,5-trihydroxyphenylalanine quinone (TPQ).

Results: The crystal structure of amine oxidase from *Escherichia coli* has been determined in both an active and an inactive form. The only structural differences are in the active site, where differences in copper coordination geometry and in the position and interactions of the redox cofactor, TPQ, are observed. Each subunit of the mushroom-shaped dimer comprises four domains: a 440 amino acid C-terminal β sandwich domain, which contains the active site and provides the dimer interface, and three smaller peripheral α/β domains (D1–D3), each of about 100 amino acids. D2 and D3 show remarkable structural and sequence similarity to each other and are conserved throughout the quinoenzyme family. In contrast, D1 is absent from some amine oxidases. The active sites are well buried from solvent and lie some 35 Å apart, connected by a pair of β hairpin arms.

Conclusions: The crystal structure of *E. coli* copper amine oxidase reveals a number of unexpected features and provides a basis for investigating the intriguing similarities and differences in catalytic mechanism of members of this enzyme family. In addition to the three conserved histidines that bind the copper, our studies identify a number of other conserved residues close to the active site, including a candidate for the catalytic base and a fourth conserved histidine which is involved in an interesting intersubunit interaction.

Structure 15 November 1995, **3**:1171–1184

Key words: amino acid derived cofactor, copper amine oxidase, quinoenzyme, 2,4,5-trihydroxyphenylalanine quinone

Introduction

Amine oxidases are important regulatory enzymes that catalyze the oxidation of a wide range of biogenic amines including many neurotransmitters, histamine and xenobiotic amines. There are two classes of amine oxidases; the flavin-containing monoamine oxidases, which have been extensively studied in eukaryotes [1], and the copper-containing amine oxidases [2–4]. The latter class has been identified in bacteria, yeasts and filamentous fungi, plants and animals, although little is known about their precise biological functions. In prokaryotic and lower eukaryotic organisms, the copper-containing amine oxidases appear to provide a route for the utilization of various amine substrates as nitrogen and carbon sources. In higher eukaryotes the situation is much less clear. In animals copper amine oxidases are implicated in development and detoxification and in plants they play roles in development, wound and resistance responses and in secondary metabolism.

Copper amine oxidases have been the subject of sustained kinetic and spectroscopic investigations [4]. They are homodimers with subunit molecular weights generally between 70 kDa and 95 kDa with one copper ion and an organic cofactor per subunit. The cofactor was initially proposed to be 2,7,9-tricarboxypyrroloquinoline quinone (PQQ) in copper amine oxidases and in several other redox-active enzymes [5]. However, the cofactor was subsequently shown to be the quinone derived from 2,4,5-trihydroxyphenylalanine (TPQ) in bovine serum amine oxidase [6] and other copper amine oxidases [7–9]. In the other proposed PQQ-containing enzymes, namely methylamine dehydrogenase and galactose oxidase, the cofactors have since been shown to be tryptophan tryptophylquinone (TTQ) [10] and 3′-*S*-cysteinyltyrosine [11], respectively. These cofactors are all formed by the post-translational modification of one or more amino acid side chains of the polypeptide chain. In the copper amine oxidases, the precursor of TPQ has been shown to be a tyrosine [7] and quinone formation is a self-processing phenomenon requiring only the copper bound in the active site of the enzyme and the presence of oxygen [8,12].

Alignments of amino acid sequence data for known copper amine oxidases show 33 totally conserved residues, representing only some 5% of the aligned residues. These conserved residues include the TXXNYD/E motif (where X is any amino acid residue) at the active site, within which the tyrosine, residue 466

*Corresponding author. MRP and MAC contributed equally to this work. †Present address: Department of Chemistry, University of Gorakhpur, Gorakhpur 273009, India.

 ISSN 0969-2126

in *Escherichia coli* amine oxidase (ECAO), is modified to TPQ. Early protein sequence alignments proved to be misleading because they included a sequence for the lentil enzyme [13] which has recently been shown to have 80 additional amino acids, including 79 residues that extend the C terminus [14].

Spectroscopic studies of amine oxidases indicate that three histidine side chains constitute the protein-derived copper ligands [3]. Because the sequence alignments only identified three fully conserved histidine residues (440, 524 and 526 in ECAO) [15–17], these residues had understandably been suggested to be the copper ligands. Following the recent re-assessment of the original lentil amine oxidase sequence, it is now clear that the C-terminal end of the copper amine oxidases is, in fact, one of the most highly conserved regions. Of the 33 conserved residues, 10 lie within a stretch of only 41 aligned residues within this region [14], and one of these conserved residues is a histidine (His689 in ECAO). The importance of the HXH motif in copper binding has been demonstrated for the *Hansenula polymorpha* enzyme by mutagenesis studies [12], but the conclusion that His440 represents the third copper ligand requires reappraisal. Indeed, the structure determination described here unambiguously identifies His689 as the third copper ligand, although the location of His440 close to the active site suggests that it too is likely to play an important role.

Copper amine oxidases catalyze the oxidation of various mono-, di- and polyamines with characteristic substrate preference depending upon the enzyme source. The reaction follows the general scheme:

$$\text{E-C=O} + \text{R-CH}_2\text{NH}_2 \rightarrow \text{E-CH-NH}_2 + \text{R-CHO} \quad (1)$$

$$\text{E-CH-NH}_2 + \text{O}_2 \rightarrow \text{E-C=O} + \text{NH}_3 + \text{H}_2\text{O}_2 \quad (2)$$

where E-C=O represents the enzyme-quinone and $\text{R-CH}_2\text{NH}_2$ is the substrate. A more detailed description of the proposed mechanism [4] is shown in Figure 1. During the reductive half-reaction (**1**), the enzyme reacts with substrate through formation of a Schiff base complex between the substrate and TPQ (species 1 in Fig. 1). Subsequent C–H bond cleavage through a proton abstraction mechanism (species 2 and 3 in Fig. 1) releases product aldehyde to leave an aminoquinol form of the enzyme (species 4 in Fig. 1). Based on pH-dependence studies of the reductive half-reaction for bovine serum amine oxidase, a general base group with low pK_a (<5) has been tentatively identified as a carboxylate group [18], although attempts at direct identification using mechanism-based inhibitors have so far proved unsuccessful. It has been reported that in lentil amine oxidase, copper is not required for the reductive half-reaction (**1**) [19].

Unlike the flavin-containing amine oxidases, where the pro-*R* proton is always abstracted, the stereochemistry of proton abstraction catalyzed by copper amine oxidases is intriguing. With simple substrates like benzylamine (Fig. 1) the pro-*S* hydrogen is always removed, while with other more physiological phenethylamine-type substrates, proton abstraction at C1 can be pro-*S*, pro-*R*, or non-stereospecific, depending on the source of the enzyme [20,21]. This property, together with variation in solvent exchange at the C2 position of the substrates, and differential rates for the reductive (**1**) and oxidative (**2**) half-reactions, points to subtle variations in the active sites of members of the enzyme family.

The oxidative half-reaction (**2**) leads to reoxidation of the aminoquinol cofactor and release of ammonia and hydrogen peroxide. The detailed mechanism of this half-cycle is poorly understood, although involvement of copper is a requirement. The Cu(II)/aminoquinol, which results from release of the product aldehyde, is proposed to be in equilibrium with a Cu(I)/semiquinone intermediate that has been detected in electron paramagnetic resonance (EPR) and rapid reaction kinetic studies [22,23]. This Cu(I)/semiquinone intermediate would react rapidly with molecular oxygen to regenerate the Cu(II)/TPQ form of the enzyme.

A more complete understanding of the molecular nature of catalysis by amine oxidases depends on the availability of atomic resolution structures for the enzyme and catalytic intermediates. Here we describe the first structure of a copper amine oxidase. *E. coli* amine oxidase is located in the periplasm and its production is stimulated greatly by providing the organism with simple aromatic amines, such as 2-phenylethylamine, as the sole source of carbon. Analysis of both an active form and an inactive form of the enzyme provides a framework for understanding how these ubiquitous quinoenzymes function.

Results and discussion

Overall molecular structure of *E. coli* amine oxidase

The ECAO dimer is mushroom-shaped (Fig. 2), with the 'stalk' comprising the first 85 amino acids of each polypeptide chain and the 'cap' the remaining 640. The N-terminal stalk domain (D1) is not present in all amine oxidases, and consists of a five-stranded antiparallel β sheet twisted around an α helix. The β sheets from the two stalk domains lie towards the molecular dyad axis, but they do not pack against each other very tightly. The interface between the two stalk domains contains several holes and buries only 420 Å^2 of solvent-accessible surface area per monomer. Only residues from the symmetry-related pair of loops between strands 1 and 2 (residues 26–29) and between strands 3 and 4 (residue 41) of the β sheets mediate direct contacts between the two stalk domains. The few interactions between the stalk domains and the remainder of the molecule are limited to those between residues 33–38, of the loop between strands 2 and 3 of D1, with residues 309–313, which form part of loop L described below.

The cap of the ECAO dimer is roughly rectangular, with dimensions 60 Å×100 Å, and 40 Å thick parallel to the molecular dyad axis. The bulk of the molecule, comprising

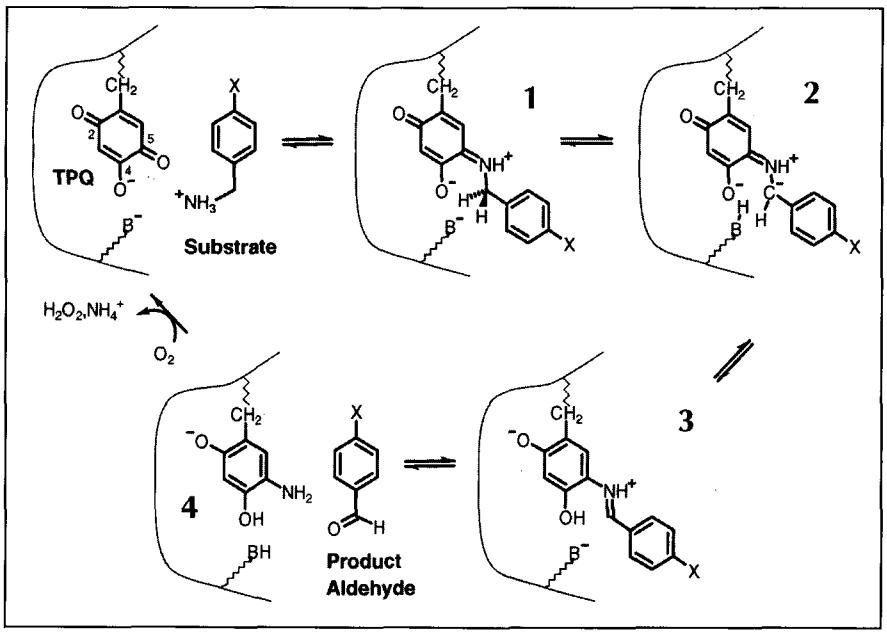

Fig. 1. Pathway for the reductive half-reaction of amine oxidase. The numbering used in describing the TPQ moiety is shown in the first panel. The substrate, shown here as a substituted phenylmethylamine, reacts with the active-site TPQ to form the substrate Schiff base (1). Abstraction of the pro-*S* proton by the general base results in a carbanionic intermediate (2) leading to the product Schiff base (3). Hydrolysis of this species releases the product aldehyde and leaves the redox cofactor in the reduced aminoquinol form (4). TPQ is regenerated by oxidation by molecular oxygen in the oxidative half-reaction.

the C-terminal 440 amino acids, folds into an extensive β sandwich (Fig. 3), which contains the active site and mediates intersubunit interactions. At the periphery of the molecule, some 30 Å from the dyad axis, each subunit has a pair of small domains (D2 and D3) comprising residues 100–185 and 186–285 respectively (Fig. 2c). A long loop of 30 amino acids, loop L (see Figs 2c,3), runs around the side and across the bottom of the cap of the molecule and connects D3 to the core β sandwich domain.

Domains D2 and D3

The domains D2 and D3 each consist of an α helix packed against a four-stranded antiparallel β sheet. Although the fold bears a superficial resemblance to that of the stalk domain, D2 and D3 are structurally distinct from D1, but display a remarkable degree of structural homology with each other. The cores of these domains (highlighted in black in Fig. 3), comprising the helix, part of the second β strand, the third and fourth β strands and the hairpin turn between them, are very similar and superimpose with a root mean square deviation (rmsd) of 0.94 Å for the main-chain atoms (Fig. 4a). Comparison of the amino acid sequences of the core regions of D2 and D3 reveals that out of 35 amino acids there are 11 identities and a further 8 conservative substitutions (Fig. 4b). The third β strand includes a run of five identical residues, AVVDL, corresponding to residues 165–169 of D2 and 266–270 of D3, for which the rmsd between the two structures is only 0.26 Å for main-chain atoms (0.65 Å for all atoms).

Extension of this comparison to the amino acid sequences of copper amine oxidases from other organisms suggests that the close similarity of domains D2 and D3 arose through a gene duplication event that must have occurred before the divergence of the different species. Because the duplicated sequences have changed so little over such an extended period of evolutionary time, the implication is that these domains have some important, yet currently unidentified, function. Although sequence and structural conservation is high within the core parts of D2 and D3, the loops that connect these conserved elements differ greatly in length and conformation.

The β sandwich domain

The central part of the ECAO dimer is made up of a pair of extensive β sandwiches that form a disk, some 60 Å in diameter and 40 Å thick. Each β sandwich is made up of one sheet with eight antiparallel strands (sheet S1), and another with ten antiparallel strands (sheet S2). Both β sheets are highly twisted, so much so that strands S2.2 and S2.9, which are topologically antiparallel (Fig. 3), run in approximately the same direction in the three-dimensional structure. In the N-terminal half of each sheet, the first five β strands follow each other in sequence, whereas the topology of the C-terminal half of each sheet is quite complex (Fig. 3). The sequence of strands is interrupted by short helices following strands S1.5, S1.8, S2.7 and S2.10, and by a small substructure (residues 491–522) comprising a turn of helix and three short antiparallel strands, termed the 'plug', which follows S2.5 (see Figs 2c,3).

The structure of the β sandwich core of ECAO appears to represent a new protein fold. A large β sandwich, comprising some 280 amino acids in antiparallel β sheets with eight and nine strands, is found in domain 5 of β-galactosidase [24] and although the two structures have similar topology in their N-terminal halves, examination of their three-dimensional structures suggests that any similarity is merely superficial. The β-galactosidase β sandwich exists as a compact globular domain and is proposed to fold as an independent module [24], whereas that in ECAO is extensively involved in the dimer interface. The ECAO β sandwich is larger than that in β-galactosidase by some 160 residues and contains more extensive regions of irregular structure as well as some very long β strands.

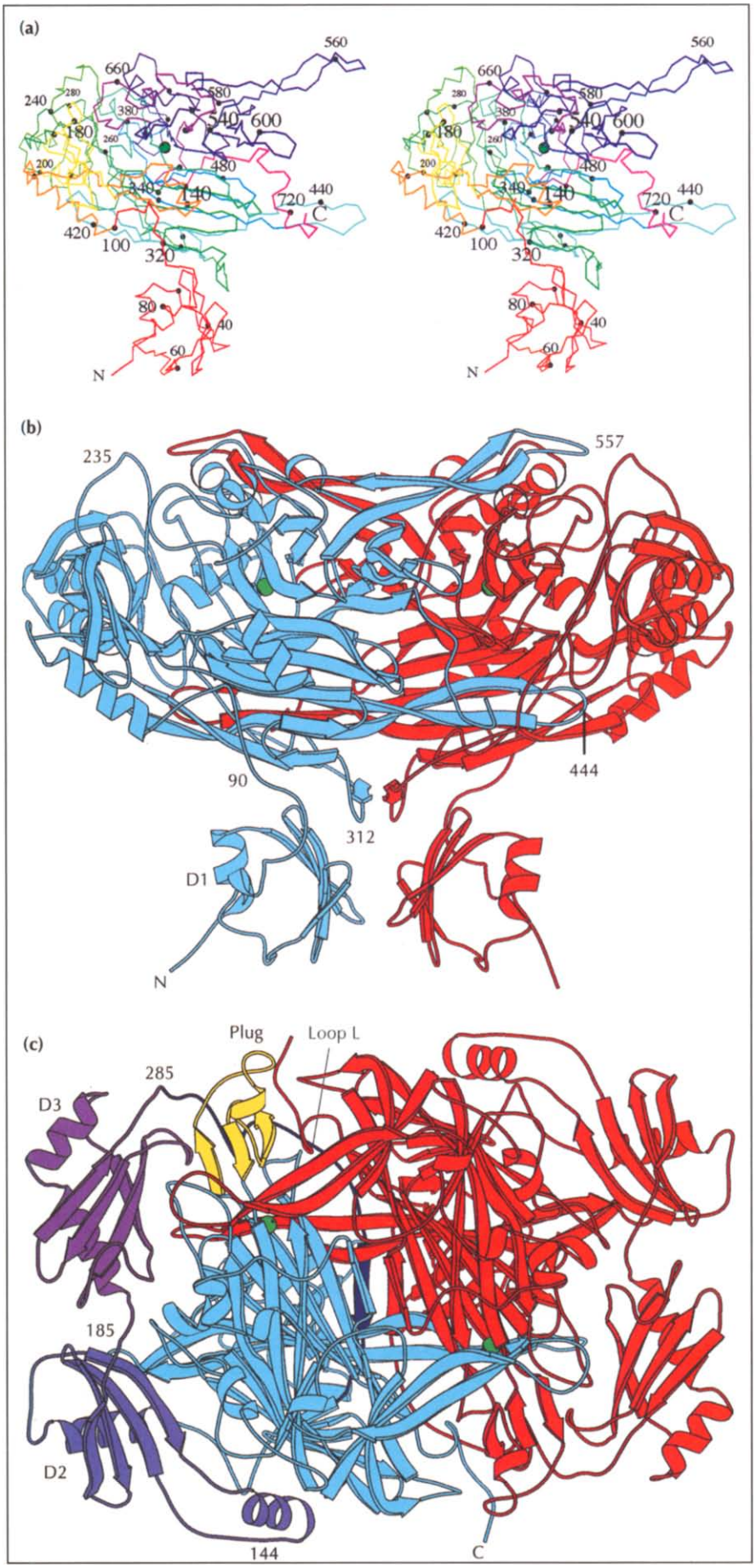

Fig. 2. Three-dimensional structure of *E. coli* amine oxidase. **(a)** Stereoview of the Cα trace of one ECAO monomer. The colour of the chain gradually changes from red at the N terminus, through yellow, green, cyan and blue to magenta at the C terminus. Every twentieth Cα atom is indicated by a small black dot and many of these bear residue numbers. The bound copper is indicated by the larger green sphere. **(b)** Ribbon diagram of the ECAO dimer viewed perpendicular to the molecular dyad axis and in the same orientation as (a). β strands are represented by flat arrows, α helices by coiled ribbons and the copper ions by small green spheres. The two subunits are coloured red and cyan. The stalk domain (D1, residues 1–85) is indicated, as are a number of residues on the cyan subunit. **(c)** A view perpendicular to (b) looking onto the 'cap', down the molecular dyad axis. One subunit is coloured red and the other is coloured to emphasize the peripheral domains: D2 (residues 101–180), blue; D3 (186–285) mauve; loop L (286–316) dark blue, and the plug substructure (491–522) yellow. The remainder of this subunit, on which a number of residues are indicated, is coloured cyan. (Figure generated using MOLSCRIPT [50].)

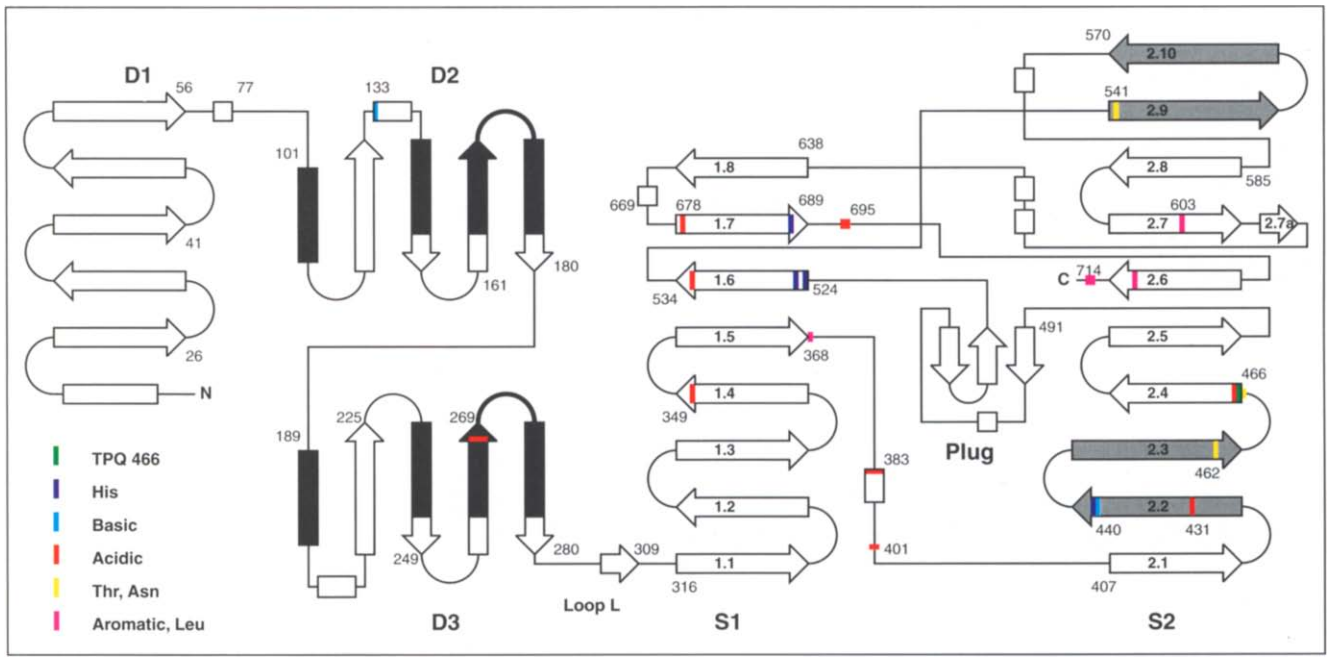

Fig. 3. Topology of a monomer of *E. coli* amine oxidase. β strands are represented by arrows and α helices by rectangles. The position of all fully conserved residues, with the exception of eight glycines and five prolines, are indicated by coloured bars, coded as shown. The following conservatively replaced polar residues are also indicated: Asp349, Asp467 and Glu695 (red) and Lys133 and Lys439 (cyan). The core regions of D2 and D3, whose main-chain atoms superimpose with an rmsd of 0.94 Å are filled in black. Within the β sandwich, the strands which make up the two sheets, S1 and S2, are labelled 1.1 to 1.8 and 2.1 to 2.10 respectively. The two β hairpin arms, S2.2/2.3 and S2.9/2.10, which embrace the other subunit are shaded grey.

Intersubunit interactions

Two pairs of adjacent strands of the larger sheet, S2.2/2.3, and S2.9/2.10, form long β hairpins or 'arms' of about 20 amino acids, that extend out of the β sandwich domain of one monomer (Fig. 2a) to embrace the other. The bound copper in one subunit lies about midway between the two arms of the other subunit (Fig. 2b). The two arms of a symmetry-related pair (S2.9/2.10) lie approximately 30 Å apart across the upper surface of the molecule with one face of the β hairpin fully exposed to solvent. The other pair of arms (S2.2/2.3) lies towards the bottom of the cap of the molecule and each arm reaches from one subunit deep into the other (Fig. 2b). Although the tips of these arms are exposed to solvent, they are each buried for most of their length by residues of loop L of the other subunit (Fig. 2c).

The second pair of arms, comprising strands S2.2 and S2.3, seems particularly important, as each arm reaches from the active site of one monomer to the active site of the other, some 35 Å away (Fig. 5). Two fully conserved residues, His440 and Thr462, lie at opposite ends of each arm (Fig. 3), such that His440 is close to one active site and Thr462 is close to the other. As detailed in the Introduction, His440 is the conserved histidine that had previously been thought to be a copper ligand.

His440 of subunit A (His440A) hydrogen bonds via Nδ1 to the side chain of Asp467B, a conserved acidic residue of the other subunit. This conserved acidic residue, which immediately follows the active-site TPQ in sequence, makes a second hydrogen bond to the side-chain hydroxyl of Thr462B. Equivalent interactions between His440B, Thr462A and Asp467A occur at the active site of the second subunit. The conserved threonine and acidic residue (Asp467) lie on either side of a β turn and are the first and last residues of the TXXNYD/E active-site motif, in which Y(466) is the tyrosine precursor to the redox cofactor, TPQ. The pair of arms with conserved residues at each end thus provide rigid structural connections between the active sites (Fig. 5). It is interesting to speculate that these may provide a mechanism for direct communication between the active sites. Cooperativity between active sites of amine oxidases has been a controversial topic [25,26] and further studies are needed to determine whether the arms connecting the active sites in ECAO have functional significance.

One result of the manner in which these two pairs of arms extend from one monomer to embrace the other is to produce an enormous area of interaction between the subunits. Some 7250 $Å^2$ of each monomer is buried in the dimer interface, corresponding to 22% of the solvent-accessible surface area of each subunit.

Although the core of each subunit is made up almost entirely of β strands, there are no extensive regions of hydrogen bonding between symmetry-related strands from the two monomers. Such interactions are limited to two short regions. Residues 609–611 form an extension to strand 2.7, named 2.7a, and interact via two pairs of equivalent hydrogen bonds with the same region from the

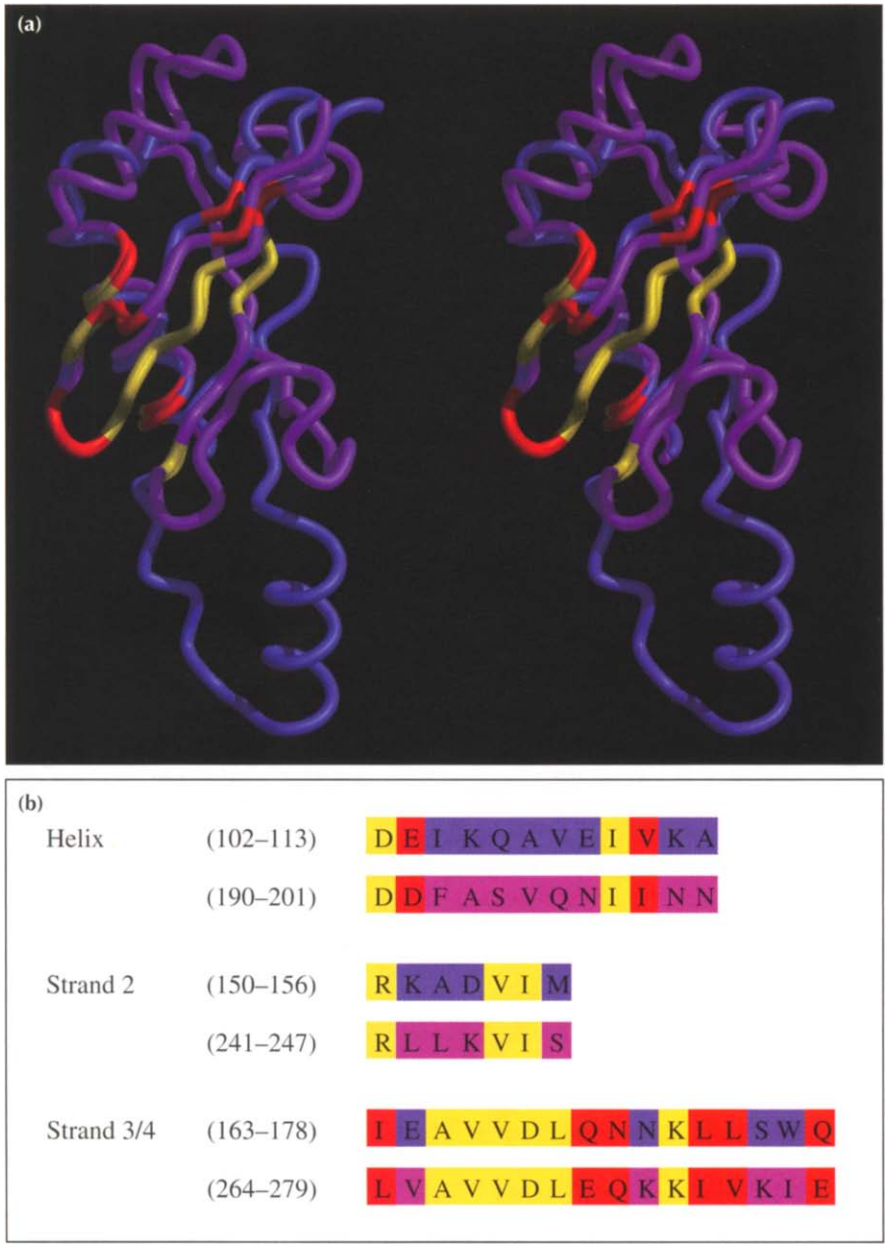

Fig. 4. Superposition of domains D2 and D3. **(a)** Stereo diagram in which the domain backbones are shown as continuous coils with D2 in blue and D3 in mauve. D3 has a similar orientation in this figure and in Figure 2c. Residues that are completely conserved between the two domains are coloured yellow and conservative changes are indicated by red. (Figure generated using MIDAS-PLUS [51].) **(b)** Sequence alignment of the core regions of peripheral domains D2 (residues 101–185, top row) and D3 (residues 186–285, bottom row) using the same colour scheme as (a).

other subunit. These strands lie in approximately the centre of the dimer interface. On the lower face of the cap of ECAO, short regions of β structure (residues 307–309) at the end of loop L of each subunit interact through a pair of equivalent hydrogen bonds close to the dyad axis.

Active-site structure

The active site itself lies between the sheets of the β sandwich, each of which contributes important residues (Fig. 6). The three histidines that act as ligands to the copper are His524 and His526 of the HXH motif, previously implicated in copper binding [12], and His689 which lies close to the C-terminal end of the sequence. These ligands lie on adjacent strands of the smaller β sheet, with His524 and His526 towards the N terminus of S1.6 and His689 at the C terminus of S1.7 (Fig. 3). TPQ is located at the N terminus of S2.4. All of the important active-site residues so far identified are well buried in the interior of the molecule. Although a number of well-ordered water molecules are found in the active site, notably one bound to O2 of TPQ, there is no channel connecting this region to bulk solvent. Much of the active-site region is buried by the plug substructure (Fig. 2c) which lies adjacent to the active site. The importance of the plug is unclear as its amino acid sequence is very poorly conserved among different species, some of which have deletions in this region of as many as 11 of the 32 residues. The closest approach of the molecular surface to the active site is at the base of a water-filled crevice which lies between the plug and residues of the upper β hairpin arm from the other subunit. The bound copper lies some 12 Å below the molecular surface and the closest ordered surface water is 14.7 Å from the copper. This crevice seems an unlikely route for entry of substrate however, as it lies on the opposite side of the copper from TPQ.

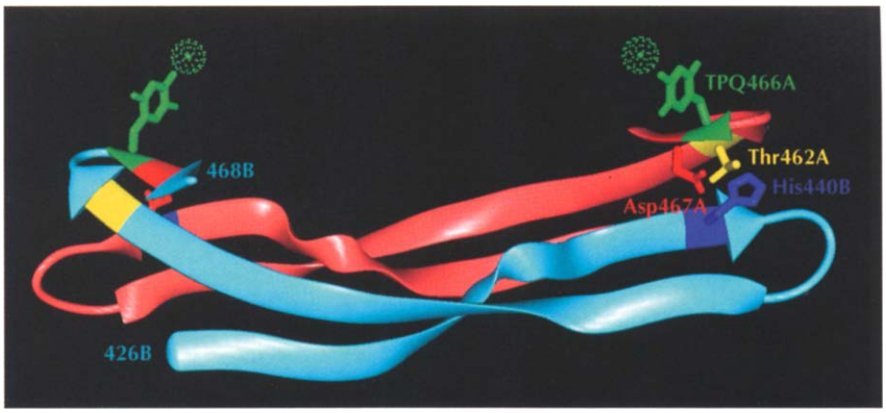

Fig. 5. Symmetry-related β hairpins linking the active sites of the ECAO monomers. β strands are shown as flat arrows coloured red in subunit A and cyan in B, as in Figure 2b. The active-site coppers are shown with van der Waals dot surfaces in green and the side chains of a number of conserved residues are in all-atom representation. Asp467A (red) and Thr462A (yellow) on either side of TPQ466A (green) both interact with His440B (blue) at the active site of subunit A and equivalent symmetry-related interactions occur at the other end of the β hairpins in the active site of subunit B.

Ammonium ions have been observed to inactivate ECAO (MJM and VB, unpublished data) by some, as yet ill defined, mechanism. Therefore, in ECAO crystal form I, which is grown from 2.3 M ammonium sulphate, the enzyme is in an inactive form. In this crystal form, the copper coordination sphere consists of the three histidines, with His524 and His526 coordinated via their Nε2 atoms and His689 via Nδ1, and TPQ466, coordinated via the oxygen at the 4-position (Fig. 7a,b). There are no water molecules bound directly to the copper. The coordination geometry is best described as distorted tetrahedral. The distortion is such that the copper lies much closer to the plane of the liganding atoms of TPQ, His526 and His689 (0.35 Å) than to any of the other faces of the tetrahedron. Inter-ligand bond angles between TPQ, His526 and His689 are in the range 105.8–127.5° whereas those from these ligands to His524 are in the range 93.3–102.4°. The distortion is thus towards trigonal bipyramidal geometry, with His524 in an 'axial-like' position and the other three ligands 'equatorial-like'. There is no electron density to suggest the presence of a second axial-like ligand; indeed there is a small empty pocket at this location, between the equatorial-like ligands and Ala486 and the side chain of Met699. Following weakly restrained refinement, copper to ligand distances are in the range 1.87–2.21 Å. The bond to His524 is slightly longer (2.18 Å, averaged over subunits A and B) than that to any of the other ligands, which average 1.94 Å to the other histidines and 2.11 Å to TPQ. A tetrahedral arrangement of copper ligands has also been reported for the type II copper site in nitrite reductase (NiR) from *Achromobacter cycloclastes* [27]. In NiR the three histidine ligands, each coordinated via Nε2, lie in a plane approximately 0.3 Å below the copper, and a water molecule above the copper completes the coordination sphere.

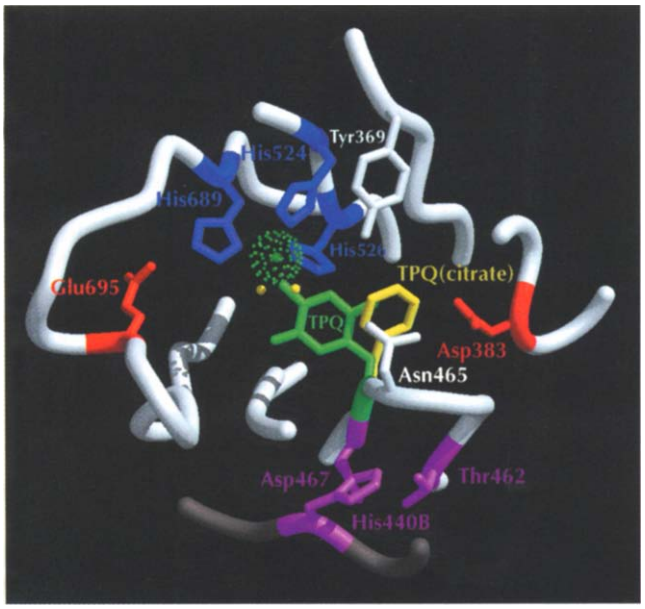

Fig. 6. Active site of *E. coli* amine oxidase. The polypeptide backbone is shown as a continuous coil, coloured white for subunit A and grey for subunit B. Conserved residues are shown in all-atom representation and the copper is shown as a green van der Waals dot surface. The position of TPQ in crystal form I is illustrated in green, coordinated to the copper. The precise location and orientation of the TPQ ring is not completely determined at the resolution of the current studies of crystal form II, and its general location is indicated by a yellow phenyl ring, close to the putative catalytic base Asp383 (red). In crystal form II, TPQ is not a copper ligand and the copper coordination is completed by two water molecules, shown in yellow. (Figures 5 and 6 generated using MIDASPLUS [51].)

Examination of conserved residues in the vicinity of the copper and TPQ (Fig. 6) suggests Asp383 as a candidate for the base required in the catalytic mechanism [18]. TPQ is oriented with O2 directed towards Asp383, although their closest approach is 5.7 Å. The active-site region contains two other conserved acidic groups: Asp467, as described above, mediates interactions between the pair of β hairpin arms that link the two active sites; and Glu695, which forms a hydrogen bond to Nε2 of the copper ligand His689, and appears to direct the other ring nitrogen (Nδ1) towards the copper. The catalytic mechanism proposed by Hartmann and Klinman [28] suggests, on chemical grounds, that substrate binding would occur at the 5-position on the TPQ ring (see Fig. 1), rather than the 2-position. In the ammonium sulphate crystal form, O5 does not lie close to any conserved residue which might be the catalytic base, but as these crystals contain inactive enzyme, the significance of the TPQ ring orientation has yet to be determined.

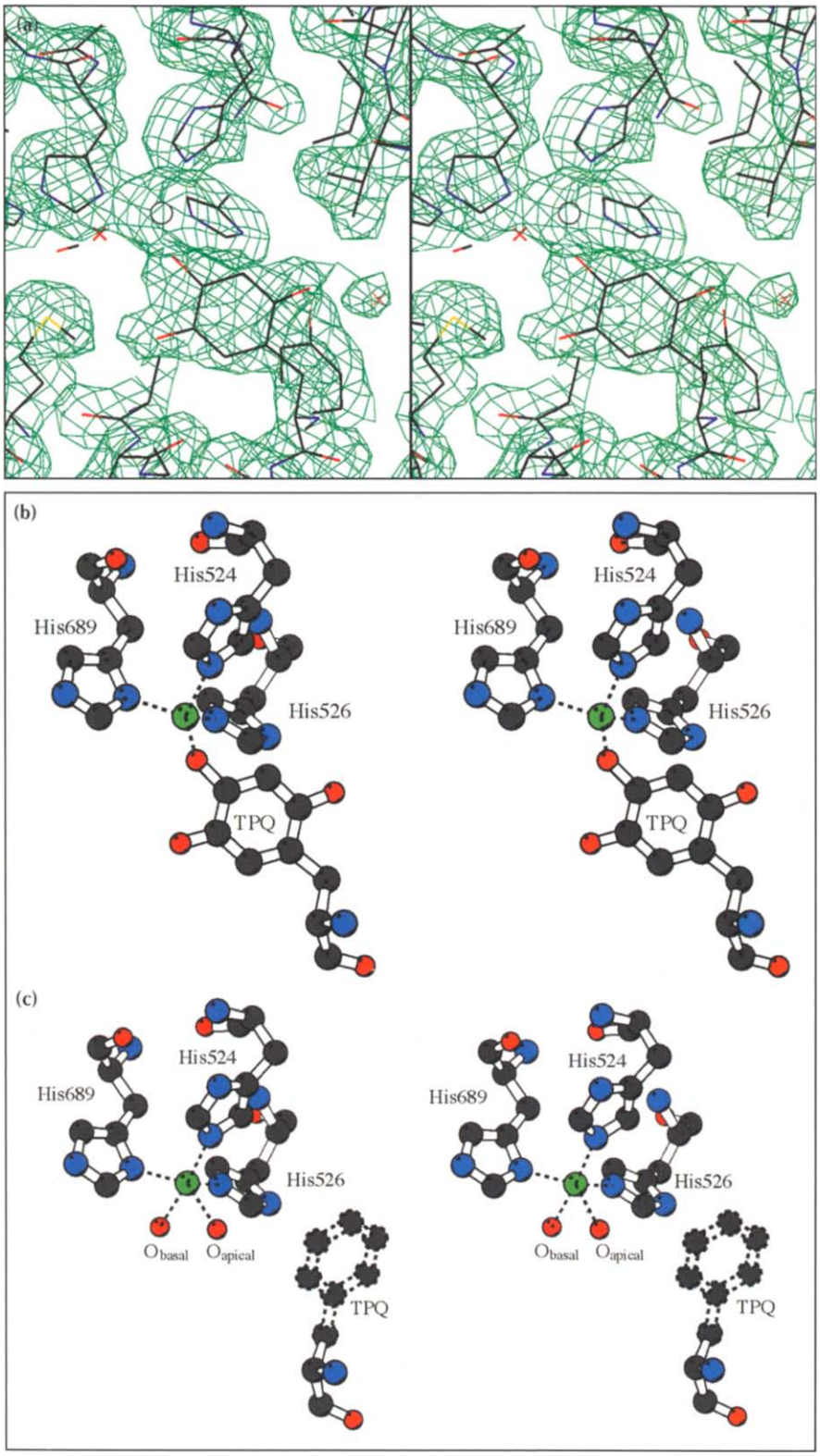

Fig. 7. Copper coordination and the active site in the two crystal forms of ECAO, viewed in the same orientation as Figure 6. **(a)** Stereo diagram of the refined atomic model in the active site of a monomer of crystal form I shown together with the final $2F_o–F_c$ electron-density map contoured at 0.8 rms. (Drawn with SKULD [N Ito, unpublished program].) **(b)** Ball-and-stick representation of the active site in crystal form I, in which the copper has distorted tetrahedral coordination. **(c)** Ball-and-stick representation of the active site in crystal form II, in which the copper has distorted square pyramidal coordination. The structures of the coppers, the liganding histidines and TPQ are shown. The general position of the TPQ, which is not a copper ligand in crystal form II, is indicated by a phenyl ring drawn in dashed lines in (c). (Parts (b) and (c) drawn with MOLSCRIPT [50].)

Structure of the active form of ECAO

ECAO crystals grown from sodium citrate solutions (form II) are not only isomorphous with crystal form I but have been shown in a coupled assay [29] (see the Materials and methods section) to exhibit catalytic activity. The ECAO structure in crystal form II has been refined at 2.4 Å and differs from form I only in the vicinity of TPQ. Although the 2.4 Å electron-density map clearly indicates the location of the TPQ side chain, there is some evidence of disorder and the ring orientation is not unequivocal. In contrast, with form I the TPQ side chain is positioned away from the copper and is not coordinated to it (Figs 6,7c) and now lies closer to the putative base, Asp383. The current map does not reveal whether O2 or O5 of TPQ lies nearest to this side chain. The difference in position of TPQ results largely

from a change of about 50° in its side chain torsion angle χ_1, which has a more favourable value in crystal form II. Small differences in position, of up to 0.3 Å, are also observed for some main-chain atoms of the TPQ residue and its immediate neighbours. The position of TPQ in form II brings O4 of TPQ within 2.5 Å of Oη of Tyr369. The relevance of any interaction between these side chains remains to be elucidated, although Tyr369 is expected to be an important residue as it is fully conserved in all known copper amine oxidase sequences.

In crystal form II, the copper has five coordinating ligands, the three histidines, coordinated as in crystal form I, and two additional water molecules (Fig. 7c). The copper and the histidine ligands from the two crystal forms superimpose very closely, although the positions of His526 differ by about 0.25 Å. The copper coordination in crystal form II is best described as distorted square pyramidal. Consistent with Jahn–Teller distortion, the apical ligand, a water molecule, lies further from the copper (2.7 Å) than the other four ligands (2.0–2.1 Å). Although two of the basal ligands, His524 and the second water, lie in positions expected for square pyramidal coordination (i.e. in a plane containing the copper and perpendicular to the apical coordination direction), His526 and His689 lie out of this plane and make inter-ligand bond angles to the apical water of 109° and 113° respectively. This distortion from regular square pyramidal towards trigonal bipyramidal presumably occurs because the histidine ligand positions are fixed by surrounding protein structure.

The copper coordination geometry in crystal form II of ECAO bears a striking similarity to that reported by Bencini *et al.* [30] for copper(II)-doped (bis[3-salicylaldiminatopropyl] methylamine)zinc(II) ([Cu,Zn]SalMeDPT). In (Cu,Zn)SalMeDPT, the arrangement of coordinating atoms in the pentadentate ligand form a distorted square pyramid, with two basal ligands making inter-ligand angles of 106° and 113° with the apical ligand. Not only are these values very similar to those for His526 and His689 in active ECAO (109° and 113°), but the polycrystalline EPR spectrum of (Cu,Zn)SalMeDPT [30] is in close agreement with that of ECAO [31]. Detailed spectroscopic studies of amine oxidases using EPR [32], nuclear magnetic relaxation [23,32], ESEEM and ENDOR [33,34], together with EXAFS [35] had indicated square pyramidal copper coordination, with three histidine ligands, grouped into two magnetically distinct populations, and with two waters, one apical and one basal. The conclusions from these spectroscopic studies are found to be in general agreement with the crystal structure of the active enzyme. In light of the inactivation of ECAO by ammonium sulphate, it is important to understand the effect of this salt on enzymes from other sources to ensure correct interpretation of spectroscopic and other physicochemical studies.

Conservation outside the active site

In addition to the coppers at the catalytic centres of ECAO, there are two other metal ions bound per monomer. These are both close to the molecular surface on the upper part of the β sandwich domain. There was no prior biochemical evidence to predict the presence of the metal-binding sites, and there is no indication that they play any role in catalysis. In each subunit, the two metal sites are 13.0 Å apart and each is about 32.5 Å from the copper. In site A, the metal ion is octahedrally coordinated by six ligands — three side-chain carboxylates, two main-chain carbonyl oxygens and a water. The metal ion in site B has pentagonal bipyramidal coordination geometry with three side-chain carboxylates, one of which is bidentate, one main-chain carbonyl, and two waters as ligands. Both metal ions have been included in the model and refined as calciums. This assignment is based on the arrangements of the ligands (three of which carry a negative charge) and on the size of the electron-density peaks.

Metal site A is almost certainly conserved in all copper amine oxidases, as two of the carboxylate metal ligands, Asp533 and Asp678, are fully conserved residues and the third, Asp535, is an acidic residue in nine out of twelve known sequences. This metal site lies at a tight turn immediately following strand S1.6 and not only do the side chains of Asp533 and Asp535 bind the metal, but the carbonyl group of the residue between them, His534, is also a ligand. The other protein ligands, namely the side chain of Asp678 and the carbonyl of Ala679, lie at the beginning of strand S1.7. Interestingly, these two antiparallel strands, S1.6 and S1.7, which have metal site A at one end, include the three conserved copper-binding histidines some ten residues away, at their other end. The three carboxylate residues in metal site B (Asp670, Glu672 and the bidentate ligand Glu573) are not completely conserved, but at least two out of three of them are acidic residues in all amine oxidase sequences except for that of *H. polymorpha*, in which only Glu672 is present.

The C-terminal 20 amino acids include five completely conserved residues, all of which are hydrophobic. These residues (Leu708, Pro710, Phe713, Phe714 and Pro718) together with Tyr603, which is also fully conserved, form a tightly packed hydrophobic cluster that lies between metal site A and the subunit interface. Another fully conserved residue from the C-terminal region of ECAO, Glu694, is also found close to this hydrophobic cluster. The side-chain carboxylate of Glu694 is buried in the dimer interface, where it makes hydrogen bonds with the main-chain amides of residues 712, 713 and 714 of the other subunit.

Conclusions

The studies of ECAO crystal structures establish the overall features of the protein and of the active site, including the ligands to the copper, the location of TPQ and identify Asp383 as the probable catalytic base. There are many features of the structure with possible functional significance which had not been identified previously including, the structural links between the two active sites, the conserved domains D2 and D3 and the additional metal-binding sites. The structural information provides a basis

both for protein engineering studies, to investigate the significance of such features, and for future crystallographic studies of substrate and inhibitor complexes of ECAO to elucidate details of the enzyme mechanism. Comparative studies of several amine oxidases are likely to be required before we will be in a position to appreciate fully the subtle differences responsible for substrate specificity, stereoselectivity and kinetic rate differences between members of the copper amine oxidase family.

Biological implications

Amine oxidases are a ubiquitous class of enzymes known to be important in cellular and extracellular metabolism of amines. In bacteria and lower eukaryotes, these enzymes provide a route for nitrogen and carbon assimilation from unusual amine sources. In animals, copper amine oxidases are extracellular and either circulating in the serum or associated with the external surfaces of cells, where they are involved in detoxification and cell signalling events. For example, a copper amine oxidase provides the major route for rapid removal from the circulation of histamine, an inflammatory and neurological regulatory molecule. It is probable that diseases found to be attributable to amine oxidase dysfunction would benefit from our ability to design novel inhibitors based on knowledge of the protein structure. In plants the role of amine oxidases is also unclear, but perhaps simpler to address as it is thought that copper amine oxidases act in regulating cell wall cross-linking, perhaps during development and in response to pathogens. Certainly, it is now accepted that hydrogen peroxide, a product of these enzymes, plays a key role in defence responses in plants.

The copper amine oxidases, such as that from *Escherichia coli*, contain a redox cofactor, 2,4,5-trihydroxyphenylalanine quinone (TPQ), which is derived by post-translational modification of tyrosine. Similar modifications have been observed in other enzymes, to generate quinones such as tryptophan tryptophylquinone [4] and other radicals derived from amino acids [36]. Thus, the range of organic chemistry available for enzyme catalysis has been extended beyond the restricted library of the standard amino acids, yet without the need for exogenous organic cofactors.

Biochemical studies have revealed that substrate amines interact directly with TPQ, forming a covalent intermediate, and the release of product aldehyde leaves the cofactor in the reduced aminoquinol form. Molecular oxygen is required to re-oxidize the cofactor. The structure of the copper amine oxidase from *E. coli* is the first reported for this class of enzyme. This structural information, in combination with the cloned gene, paves the way for protein engineering studies to explore the catalytic mechanism of *E. coli* amine oxidase, in particular the role of copper in the oxidative half-reaction. The structure of *E. coli* amine oxidase will facilitate the determination of the structures of eukaryotic amine oxidases, leading to studies of their catalytic mechanisms, which are known to differ in stereospecificity of proton abstraction [20,21].

Materials and methods

Gene amplification, cloning and sequencing

The *E. coli* amine oxidase gene was amplified from genomic DNA using the polymerase chain reaction (PCR) with oligonucleotide primers designed from published gene sequence information [37]. The primer sequences were 5′-CTGAC-GAGG*A*TCCTAATGGGAAGC-3′, which included three base changes (shown in italics) from the published sequence to incorporate a unique *Bam*HI site (underlined), and 5′-GTTTTTTTGTCTGCAGCAATCACTTATC-3′, with two base changes to incorporate a unique *Pst*I site. The PCR mix (10 μl) contained 60 ng genomic DNA, 10 pmole of each primer, 10 mM Tris-HCl, pH 9.0, 50 mM KCl, 0.1% (w/v) gelatin, 2.25 mM $MgCl_2$, 0.1% Triton X-100, 0.2 mM dNTPs, 0.25 ng ml^{-1} bovine serum albumin and 0.5 units of SuperTaq (Stratech Scientific Ltd., Luton, Beds, UK) and was sealed in a glass capillary. The amplification was performed in an Idaho Technologies Air-Thermal-Cycler (Idaho Technologies, Idaho Falls, ID) using the program: initial denaturation at 95°C for 30 s, followed by 35 cycles of (95°C, 0 s; 55°C, 0 s; 72°C, 45 s) with a final extension step at 72°C for 90 s.

The resulting PCR product (2.18 kb) was fractionated through a 1.0% agarose gel and isolated in a gel slice from which the DNA was recovered by centrifugation through glass wool [38]. The DNA was then extracted with phenol:chloroform (50:50 v/v) and concentrated by ethanol precipitation [39]. The purified 2.2 kb PCR fragment was ligated into the vector pCRII as detailed for the TA Cloning kit (Invitrogen Corporation, San Diego, CA). Plasmid pEC1 was recovered following transformation of *E. coli* INVαF′ (Invitrogen).

Plasmid pEC1 DNA was purified using a Qiagen (Qiagen Inc., Chatsworth, CA) maxiprep plasmid purification kit. Manual sequencing was performed using a Sequenase version 2.0 sequencing kit (Amersham International plc, Aylesbury, Bucks, UK). Automated DNA sequence data were obtained with a PRIZM Ready Reaction DyeDeoxy terminator cycle sequencing kit (Perkin–Elmer, Beaconsfield, Bucks, UK) and sample analysis on an Applied Biosystems 373A automated sequencing instrument (Perkin–Elmer). Sequence information obtained from pEC1 clones derived from independent PCR experiments was compiled for both strands of the gene using the nucleotide fragment assembly programs of the GCG Package (Genetics Computer Group, Madison, Wisconsin). The nucleotide sequence data have been submitted to Genbank under accession number L47571. Comparison of the translated amino acid sequences of the amine oxidase gene cloned during the present study with that reported previously [37] reveals several differences, as shown in Table 1.

Protein purification and enzyme assay

E. coli were grown overnight at 30°C in M63 minimal salts medium containing 5 mM β-phenylethylamine and 1 μM $CuSO_4$. When the OD_{680} had reached 0.4–0.6 the cultures

Table 1. Amino acid differences between the present and published [37] sequences of *E. coli* amine oxidase (ECAO).

Residue number	ECAO residue (this study)	ECAO residue Ref. [37]
218	Lysine	Glutamate
228	Glycine	Valine
229	Tyrosine	Isoleucine
between 245 and 246	none	Isoleucine
258	Alanine	none
260	Proline	Isoleucine
426	Alanine	Proline
629	Histidine	Aspartate

All numbering refers to the coding region of the mature protein as determined during this study. Relative to the present determination, the previously published sequence has a residue inserted between amino acids 245 and 246, and a deletion at amino acid 258, in addition to six amino acid substitutions.

were chilled on ice and then harvested by centrifugation (Sorval SS34 (Dupont [UK] Ltd., Stevenage, Herts, UK), 5 min, 7000 rpm at 4°C). All procedures for preparation of periplasmic fractions were performed at 0°C. The periplasmic fraction, which contained the copper amine oxidase, was prepared essentially according to Cooper *et al.* [31]. The proteinase inhibitors *N*-tosyl-L-phenylalanine chloromethyl ketone (TPCK) and phenylmethylsulphonyl fluoride (PMSF) were then included at final concentrations of 43 μg ml^{-1} and 870 μg ml^{-1} respectively. Biochemical studies of ECAO (MJM and VB, unpublished data) have shown that the enzyme is inactivated by exposure to ammonium ions. In order to prepare fully active enzyme, the previously reported protein purification protocol [31] was modified to exclude ammonium sulphate. The periplasmic fraction was concentrated using an Amicon concentrator (Amicon Ltd., Stonehouse, Gloucs, UK) rather than by ammonium sulphate precipitation. Following extensive dialysis against 20 mM Tris-HCl, pH 7.0 and further concentration using the Amicon concentrator, the sample was fractionated by FPLC through a 20 ml Q-Sepharose Hi-Load column (Pharmacia Biotech Ltd., St. Albans, Herts, UK). Protein was eluted with a gradient of 20 mM Tris-HCl, pH 7.0 containing 0–0.185 M NaCl at a flow rate of 2 ml min^{-1}. Peak active fractions were concentrated using an Amicon concentrator and loaded directly onto an Ultra-gel AcA 34 column (LKB) (1.6×100 cm containing 200 ml bed volume). The proteins were separated on the column at a flow rate of ~8 ml 20 mM Tris-HCl, pH 7.0 per hour. Fractions containing purified enzyme were identified by SDS-PAGE and enzyme assay and were then concentrated to 4–5 mg ml^{-1}. For crystallographic studies enzyme samples were used immediately, otherwise the protein was stored as aliquots in a liquid nitrogen store.

A coupled enzyme assay system was used, based on the method of Amaral *et al.* [29], in which amine oxidase-mediated oxidation of the substrate β-phenylethylamine generates hydrogen peroxide for use by horseradish peroxidase to oxidize a colourless substrate to a coloured product. The reagent mix was prepared by adding 5 mg horseradish peroxidase, 10 mg β-phenylethylamine and 25 mg 2,2′-azino-bis(3-ethylbenzthiazoline)-6 sulphonic acid (ABTS) to 25 ml of 100 mM sodium phosphate buffer, pH 7.0. Activity was recorded at 30°C as the change in absorbance at 410 nm in reaction volumes of 1 ml reagent mix. Specific activities were determined as μmol H_2O_2 generated per minute assuming ϵ=29300 for ABTS. Assays of amine oxidase activity in the crystals were performed by adding components of the ABTS assay mix to a crystal washed and stabilized in the crystallization medium. Colour change was visually monitored by microscopic examination. After 15 min, a green colour was observed in the assay mix containing a crystal grown from sodium citrate (crystal form II), whereas that containing a crystal from ammonium sulphate (crystal form I) remained colourless. For detection of active enzyme in a non-denaturing polyacrylamide gel, a similar reagent mix was used except that 17 mg diaminobenzidine (DAB) was used in place of the ABTS. The gel was immersed in the reagent mix until bands were visible and the gel was then washed in distilled water. The DAB product is insoluble and so remains localized to the active enzyme band in the gel.

Structure determination of crystal form I

Crystals of ECAO were grown from solutions containing 2.3 M ammonium sulphate, 100 mM HEPES pH 7.0, by the vapour diffusion method. They form as elongated rods (0.3×0.3×0.6 mm^3) in the space group $P2_12_12_1$ with unit cell dimensions a=135.6 Å, b=167.8 Å, c=81.5 Å. The crystals contain a dimer in the asymmetric unit, with a solvent content of 55%.

Data to 2.8 Å resolution were recorded from native and derivative crystals using a Siemens multiwire area detector mounted on a Rigaku RU-200 generator, with a rotating copper anode and a 200 μm focus, run at 45 kV, 60 mA. Data were processed with XDS [40] and all subsequent merging and scaling was performed using programs from the CCP4 program suite [41]. Native data to beyond 2.0 Å resolution were recorded with a large MAR image plate at Station 9.6, Daresbury SRS, at wavelength 0.89 Å. The 2.4 Å citrate-grown form II data were collected in the same way. Data to 2.5 Å resolution were recorded from the trimethyl lead acetate (TMLA) derivative with a large MAR image plate detector at the tuneable beamline Station 9.5, Daresbury SRS, using X-rays with a wavelength of 0.93 Å, chosen to optimize anomalous scattering from lead. A partial 2.5 Å data set was also recorded from the niobium derivative at Station 9.5. All image plate data were processed with MOSFLM [42]. The area detector and SRS derivative data sets showed different heavy-atom occupancies so all the data sets were retained in the phase calculation. Data collection statistics are summarized in Table 2.

Initial phases were obtained using the multiple isomorphous replacement method with two principal derivatives: Nb_6Cl_{14} and TMLA. Three niobium cluster sites were located using direct methods in SHELXS-86 [43]. Four TMLA sites and a fourth niobium cluster were located in difference Fourier maps. Heavy-atom parameters were refined in MLPHARE [41]. The niobium clusters were treated as single atoms with temperature factors (B) of 150 $Å^2$ for data in the resolution range 20.0–6.0 Å, and as octahedral clusters of six niobium atoms, with temperature factors of 30 $Å^2$, for data from 4.5–2.5 Å. Initial orientations of the clusters were estimated from the shapes of the peaks in a TMLA-phased difference Fourier map. Although the niobium derivative made an important contribution to phasing at low resolution, high-resolution phasing was dominated by the TMLA derivative. The mean figure of merit for all phases to 2.5 Å was 0.36.

The non-crystallographic dyad axis was located from analysis of the coordinates of the four TMLA sites and was consistent with peaks in native and TMLA derivative self-rotation functions. The 6.0 Å MIRAS map was skewed into the molecular

Table 2. Data collection and heavy-atom refinement statistics.

Crystal*	Source	dmin (Å)	Number of measurements	Multiplicity	Completeness (%)	Number of crystals	R_{symm}# (%)	R_{deriv}** (%)	Phasing power††
Native (form I)	SRS	2.0	435398	3.7	90.5	10	6.9	–	–
TMLA	RU-200	2.8	76849	2.0	80.4	1	6.5	15.5	1.34
TMLA	SRS	2.5	153230	2.5	86.5	6	6.4	13.8	1.04
Nb6	RU-200	6.0†	58878	2.8	86.6	1	5.6	15.8	1.67
Nb6	SRS	2.5	39585	1.4	43.9§	2	7.3	27.3	0.68
Nb6	SRS	6.0‡	ND	ND	ND	2	ND	ND	2.4
W12	RU-200	6.0	25423	4.4	99.7	1	5.8	9.7	0.46
Native (form II)	SRS	2.4	180978	2.7	90.7	4	8.0	–	–

*Heavy-atom derivatives as follows: TMLA, 10 mM trimethyl lead acetate; Nb6, saturated Nb_6Cl_{14} (~ 0.5 mM); W12, 1 mM $H_3PO_4.12WO_3$. †The figure quoted is for data processed to 3.5 Å but only data to 6.0 Å were used in phasing. ‡This is the same data set as above, but in heavy-atom refinement and phasing the clusters are treated as single sites and data used to 6.0 Å only. §Due to lack of beam time, the Nb6 SRS data set comprises only 25° (out of the required 90°) of data frames. As a result, heavy-atom parameters refined using these data were treated with caution, although their inclusion in phasing did result in a small improvement in figure of merit. #$R_{symm}=\Sigma_h|I(h)-\langle I(h)\rangle|/\Sigma_h|I(h)|$. **$R_{deriv}=\Sigma_h|F(h)_{native}-F(h)_{deriv}|/\Sigma_h|F(h)|$. ††Phasing power=$\langle F_H/|F_{PH}-|F_P+F_H||\rangle$.

coordinate frame and averaged about the molecular dyad axis with SKEWPLANES [44]. A solvent envelope was drawn by hand onto sections of the averaged skewed map using a procedure based on the graphical program Xfig (S Sutanthavibul, Univ. of Texas, Austin) and a three-dimensional solvent mask was generated with modified programs from the ENGENE package [45]. After back-transformation into the crystallographic coordinate frame this solvent mask was used, along with twofold molecular averaging, to improve the phases (new figure of merit 0.77) using DM [46].

Model building and refinement

Skeletonization of the resulting 2.5 Å map using BONES [47] formed the basis for an initial polyalanine trace of 250 residues of the core β sheet structure. The quality of the electron density allowed some distinctive patterns of side chains to be identified, the sequence to be assigned (see Table 1) and the model extended using FRODO [48]. The second subunit was initially generated using non-crystallographic symmetry, but in the subsequent refinement, phase extension to 2.0 Å and model rebuilding, the two subunits were treated independently.

The molecular structure was subjected to restrained least-squares refinement of atomic positions and thermal parameters in PROLSQ [41], using all data in the resolution range 8.0–2.0 Å. The final model contains residues 5–727 of each subunit, one copper and two bound cations per monomer, and 1033 ordered water molecules (Table 3). Excluding the glycines and prolines, 1105 out of 1234 residues (89.5 %) lie in the most favoured regions of the Ramachandran plot and four residues, 35A, 326A, 182B and 326B, lie in disallowed regions.

The two subunits superimpose with an rmsd for all main-chain atoms of the entire molecule of 0.546 Å and with an rmsd of 0.280 Å for all main-chain atoms in the cap (residues 86–727). The rms fit of the stalk regions (residues 5–85) is 0.464 Å, indicating that the two domains D1, although very similar in structure, have slightly different orientations with reference to the remainder of their respective subunits. Refined ECAO coordinates from crystal form I have been submitted to the Brookhaven Protein Data Bank (code 1OAC).

During refinement, the metal–ligand distances were restrained to appropriate values derived from small-molecule structures. In order to examine the copper coordination geometry in more detail, the final model was subjected to further cycles of refinement in which all geometric restraints were relaxed by a factor of 33. The rms movement of the coppers and ligands during this weakly restrained refinement was 0.14 Å.

Structure determination of crystal form II

As the crystal form described above (crystal form I) was grown from ammonium sulphate solutions, the structure is that of the inactivated enzyme. In order to determine whether the inactive enzyme differs in structure from its active form we have also prepared crystals of fully active ECAO from sodium citrate solutions (1.4 M sodium citrate, 100 mM HEPES buffer, pH 7.0: crystal form II), using conditions based on those reported by Roh *et al.* [49]. ECAO has been shown to be active in crystal form II with phenylethylamine as the substrate (see above).

Crystals of form II are isomorphous with crystal form I, although their smaller size has so far limited data collection to

Table 3. Summary of refinement of ECAO.

Crystal form	Total number of protein atoms	Total number of waters	Resolution range	Reflections	R factor*	Cut-off	Rmsd bonds	Rmsd angles	B factors†
I	11366	1031	8.0–2.0 Å	108803	15.9%	none	0.012 Å	0.041 Å	2.821 Å^2
				101778	15.0%	$F_o>3\sigma F_o$			
II	11305	979	10.0–2.4Å	63566	14.5%	none	0.014 Å	0.048 Å	3.423 Å^2
				59326	13.8%	$F_o>3\sigma F_o$			

*R factor=$\Sigma_h|F_o(h)-F_c(h)|/\Sigma_h F_o(h)$. †For bonded main-chain atoms.

2.4 Å resolution. A preliminary $F_{obs(form\ II)}-F_{obs(form\ I)}$ difference Fourier map, using phases calculated from the refined ECAO (form I) model showed that the only major structural change was in the position of the TPQ side chain. The position of the basal water, some 2.0 Å from the copper, was clear as a peak of greater than six times the rms density of this map. Starting from the refined ECAO model from crystal form I, but with both TPQs replaced by alanines, ECAO has been refined against all form II data in the resolution range 10.0–2.4 Å, to an R factor of 14.5%. After five cycles of refinement, the apical water was also identified, at a distance of 2.8 Å from the copper, and was included in the model. The refined model includes residues 7A–724A, 7B–725B and 979 waters (Table 3). Due to the relatively poor ratio of observations to parameters (Table 3), ECAO form II has not been subjected to refinement with the same loose restraints as form I.

Acknowledgements: We thank RA Cooper and JP Porter for help in the early stages of the protein purification, JN Keen for N-terminal sequencing of the protein, D Ashworth for automated DNA sequencer operation and JP Klinman for discussions on the enzyme mechanism. We wish to thank E Duke, P Rizhkallah and the staff of Daresbury SRS for help with data collection and processing, BW Matthews for providing β-galactosidase coordinates and D Dixon for assistance in preparing the figures. BBSRC and EPSRC provided support for this research, including a Senior Visiting Fellowship to KDSY. SEVP is an International Scholar of the Howard Hughes Medical Institute and MJM was a Leverhulme Trust/Royal Society Senior Research Fellow.

References

1. Berry, M.D., Juorio, A.V. & Paterson, I.A. (1994). The functional role of monoamine oxidase-A and oxidase-B in the mammalian central nervous system. *Prog. Neurobiol.* **42**, 375–391.
2. McIntire, W.S. & Hartmann, C. (1993). Copper-containing amine oxidases. In *Principles and Applications of Quinoproteins.* (Davison, V.L., ed), pp. 97–171, Marcel Dekker, New York.
3. Knowles, P.F. & Dooley, D.M. (1994). Amine oxidases. In *Metal Ions in Biological Systems.* (Sigel, H. & Sigel, A., eds), vol. **30**, pp. 361–403, Marcel Dekker, New York.
4. Klinman, J.P. & Mu, D. (1994). Quinoenzymes in biology. *Annu. Rev. Biochem.* **63**, 299–344.
5. Duine, J.A. & Jongejan, J.A. (1989). Quinoproteins, enzymes with pyrrolo-quinoline quinone as cofactor. *Annu. Rev. Biochem.* **58**, 403–426.
6. Janes, S.M., *et al.*, & Klinman, J.P. (1990). A new redox cofactor in eukaryotic enzymes: 6-hydroxydopa at the active-site of bovine serum amine oxidase. *Science* **248**, 981–987.
7. Mu, D., Janes, S.M., Smith, A.J., Brown, D.E., Dooley, D.M. & Klinman, J.P. (1992). Tyrosine codon corresponds to topa quinone at the active site of copper amine oxidases. *J. Biol. Chem.* **267**, 7979–7982.
8. Matsuzaki, R., Fukui, T., Sato, H., Ozaki, Y. & Tanizawa, K. (1994). Generation of the topa quinone cofactor in bacterial monoamine oxidase by cupric ion-dependent autooxidation of a specific tyrosyl residue. *FEBS Lett.* **351**, 360–364.
9. Janes, S.M., *et al.*, & Klinman, J.P. (1992). Identification of topaquinone and its consensus sequence in copper amine oxidases. *Biochemistry* **31**, 12147–12154.
10. McIntire, W.S., Wemmer, D.E., Chistoserdov, A. & Lidstrom, M.E. (1991). A new cofactor in a prokaryotic enzyme: tryptophan tryptophylquinone as the redox prosthetic group in methylamine dehydrogenase. *Science* **252**, 817–824.
11. Ito, N., *et al.*, & Knowles, P.F. (1991). Novel thioether bond revealed by a 1.7 Å crystal structure of galactose oxidase. *Nature* **350**, 87–90.
12. Cai, D. & Klinman, J.P. (1994). Copper amine oxidase: heterologous expression, purification, and characterization of an active enzyme in *Saccharomyces cerevisiae. Biochemistry* **33**, 7647–7653.
13. Rossi, A., Petruzzelli, R. & Agro, A.F. (1992). cDNA-derived amino acid sequence of lentil seedlings amine oxidase. *FEBS Lett.* **301**, 253–257.
14. Tipping, A.J. & McPherson, M.J. (1995). Cloning and molecular analysis of the pea seedling copper amine oxidase. *J. Biol. Chem.* **270**, 16939–16946.
15. Zhang, X.P., Fuller, J.H. & McIntire, W.S. (1993). Cloning, sequencing, expression, and regulation of the structural gene for the copper/topa quinone-containing methylamine oxidase from *Arthrobacter* strain P1, a gram-positive facultative methylotroph. *J. Bacteriol.* **175**, 5617–5627.
16. Mu, D., *et al.*, & Klinman, J.P. (1994). Primary structures for a mammalian cellular and serum copper amine oxidase. *J. Biol. Chem.* **269**, 9926–9932.
17. Choi, Y.H., *et al.*, & Tanizawa, K. (1995). Copper topa quinone containing histamine oxidase from *Arthrobacter globiformis* — molecular cloning and sequencing, overproduction of precursor enzyme, and generation of topa quinone cofactor. *J. Biol. Chem.* **270**, 4712–4720
18. Farnum, M., Palcic, M. & Klinman, J.P. (1986). pH-dependence of deuterium isotope effects and tritium exchange in the bovine plasma amine oxidase reaction — a role for single base catalysis in amine oxidation and imine exchange. *Biochemistry* **25**, 1898–1904.
19. Rinaldi, A., Giartosio, A., Floris, G., Medda, R. & Agro, A.F. (1984). Lentil seedlings amine oxidase — preparation and properties of the copper-free enzyme. *Biochem. Biophys. Res. Commun.* **120**, 242–249.
20. Scaman, C.H. & Palcic, M.M. (1992). Stereochemical course of tyramine oxidation by semicarbazide sensitive amine oxidase. *Biochemistry* **31**, 6829–6841.
21. Coleman, A.A., Scaman, C.H., Kang, Y.J. & Palcic, M.M. (1991). Stereochemical trends in copper amine oxidase reactions. *J. Biol. Chem.* **266**, 6795–6800.
22. Bellelli, A., Agro, A.F., Floris, G. & Brunori, M. (1991). On the mechanism and rate of substrate oxidation by amine oxidase from lentil seedlings. *J. Biol. Chem.* **266**, 20654–20657.
23. Dooley, D.M., McGuirl, M.A., Brown, D.E., Turowski, P.N., McIntire, W.S. & Knowles, P.F. (1991). A Cu(I)-semiquinone state in substrate reduced amine oxidases. *Nature* **349**, 262–264.
24. Jacobson, R.H., Zhang, X.J., Dubose, R.F. & Matthews, B.W. (1994). Three-dimensional structure of beta-galactosidase from *Escherichia coli. Nature* **369**, 761–766.
25. Janes, S.M. & Klinman, J.P. (1991). An investigation of bovine serum amine oxidase active site stoichiometry — evidence for an aminotransferase mechanism involving 2 carbonyl cofactors per enzyme dimer. *Biochemistry* **30**, 4599–4605.
26. Agostinelli, E., Morpurgo, L., Wang, C.Q., Giartosio, A. & Mondovi, B. (1994). Properties of cobalt-substituted bovine serum amine oxidase. *Eur. J. Biochem.* **222**, 727–732.
27. Godden, J.W., *et al.*, & Legall, J. (1991). The 2.3 angstrom X-ray structure of nitrite reductase from *Achromobacter cycloclastes. Science* **253**, 438–442.
28. Hartmann, C. & Klinman, J.P. (1991). Structure–function studies of substrate oxidation by bovine serum amine oxidase — relationship to cofactor structure and mechanism. *Biochemistry* **30**, 4605–4611.
29. Amaral, D., Bernstein, L., Morse, D. & Horecker, B.L. (1963). Galactose oxidase of *Polyporus cincinatus*: a copper enzyme. *J. Biol. Chem.* **238**, 2281–2284.
30. Bencini, A., Bertini, I., Gatteschi, D. & Scozzafava, A. (1978). Single-crystal ESR spectra of copper(II) complexes with geometries intermediate between a square pyramid and a trigonal bipyramid. *Inorg. Chem.* **17**, 3194–3197.
31. Cooper, R.A., Knowles, P.F., Brown, D.E., McGuirl, M.A. & Dooley, D.M. (1992). Evidence for copper and 3,4,6-trihydroxyphenylalanine quinone cofactors in an amine oxidase from the gram-negative bacterium *Escherichia coli* K-12. *Biochem. J.* **288**, 337–340.
32. Barker, R., *et al.*, & Knowles, P.F. (1979). Properties of cupric ions in benzylamine oxidase from pig plasma as studied by magnetic resonance and kinetic methods. *Biochem. J.* **177**, 289–302.
33. Baker, G.J., Knowles, P.F., Pandeya, K.B. & Rayner, J.B. (1986). Electron nuclear double resonance (ENDOR) spectroscopy of amine oxidase from pig plasma. *Biochem. J.* **237**, 609–612.
34. McCracken, J., Peisach, J. & Dooley, D.M. (1987). Cu(II) coordination chemistry of amine oxidases — pulsed electron paramagnetic res studies of histidine imidazole, water, and exogenous ligand coordination. *J. Am. Chem. Soc.* **109**, 4064–4072.
35. Scott, R.A. & Dooley, D.M. (1985). X-ray absorption spectroscopic studies of the copper(II) sites in bovine plasma amine oxidase. *J. Am. Chem. Soc.* **107**, 4348–4350.
36. Stubbe, J.A. (1989). Protein radical involvement in biological catalysis. *Annu. Rev. Biochem.* **58**, 257–285.
37. Azakami, H., Yamashita, M., Roh, J.H., Suzuki, H., Kumagai, H. & Murooka, Y. (1994). Nucleotide sequence of the gene for monoamine-oxidase (MAOA) from *Escherichia coli. J. Ferment. Bioeng.* **77**, 315–319.
38. Tautz, D. & Renz, M. (1983). An optimized freeze-squeeze method for the recovery of DNA fragments from agarose gels. *Anal. Biochem.* **132**, 14–19.

39. Sambrook, J., Fritsch, E.F. & Maniatis, T. (1989) *Molecular Cloning: A Laboratory Manual.* (2nd edn), Cold Spring Harbor Laboratory, Cold Spring Harbor, New York.
40. Kabsch, W. (1988). Automatic indexing of rotation diffraction patterns. *J. Appl. Cryst.* **21**, 67–71.
41. Collaborative Computational Project Number 4. (1994). The CCP4 suite — programs for protein crystallography. *Acta Cryst. D* **50**, 760–763.
42. Leslie, A.G.W. (1992). Recent changes to the MOSFLM package for processing film and image plate data. In *Joint CCP4 and ESF-EACBM Newsletter on Protein Crystallography, Number 26.* SERC Daresbury Laboratory, Warrington, UK.
43. Robinson, W. & Sheldrick, G.M. (1988). SHELX. In *Crystallographic Computing 4: Techniques and New Technologies.* (Isaacs, N.W. & Taylor, M.R., eds), pp. 366–377, Oxford University Press, New York.
44. Bricogne, G. (1976). Methods and programs for direct-space exploitation of geometric redundancies. *Acta Cryst. A* **32**, 832–847.
45. Cherfils, J. & Dumas, C. (1988). MEDIT — an interactive graphics editor for molecular envelopes. *J. Appl. Cryst.* **21**, 985–987.
46. Cowtan, K. (1994). DM: an automated procedure for phase improvement by density modification. In *Joint CCP4 and ESF-EACBM Newsletter on Protein Crystallography, Number 31.* pp. 34–38, SERC Daresbury Laboratory, Warrington, UK.
47. Greer, J. (1985). Computer skeletonization and automatic electron-density map analysis. *Methods Enzymol.* **115**, 206–224.
48. Jones, T.A. (1978). A graphics model building and refinement system for macromolecules. *J. Appl. Cryst.* **11**, 268–272.
49. Roh, J.H., *et al.*, & Mikami, B. (1994). Crystallization and preliminary X-ray analysis of copper amine oxidase from *Escherichia coli* K-12. *J. Mol. Biol.* **238**, 635–637.
50. Kraulis, P.J. (1991). MOLSCRIPT: a program to produce both detailed and schematic plots of protein structures. *J. Appl. Cryst.* **24**, 946–950.
51. Ferrin, T.E., Huang, C.C., Jarvis, L.E. & Langridge, R. (1988). The MIDAS display system. *J. Mol. Graphics* **6**, 13–27.

Received: **8 Sep 1995**; revisions requested: **20 Sep 1995**; revisions received: **27 Sep 1995**. Accepted: **27 Sep 1995**.